Turbulent and neoclassical impurity transport in tokamak plasmas

T. Fülöp and H. Nordman
Department of Radio and Space Science, Chalmers University of Technology and Euratom-VR Association, Göteborg SE-41296, Sweden

(Received 22 December 2008; accepted 28 January 2009; published online 12 March 2009)

Impurity particle transport in tokamaks is studied using an electrostatic fluid model for main ion and impurity temperature gradient (ITG) mode and trapped electron (TE) mode turbulence in the collisionless limit and neoclassical theory. The impurity flux and impurity density peaking factor obtained from a self-consistent treatment of impurity transport are compared and contrasted with the results of the often used trace impurity approximation. Comparisons between trace and self-consistent turbulent impurity transport are performed for ITER-like profiles. It is shown that for small impurity concentrations the trace impurity limit is adequate if the plasma is dominated by ITG turbulence. However, in case of TE mode dominated plasmas the contribution from impurity modes may be significant, and therefore a self-consistent treatment may be needed. © *2009 American Institute of Physics*. [DOI: 10.1063/1.3083299]

I. INTRODUCTION

Fusion performance is expected to be significantly affected by impurities that contribute to radiation losses and plasma dilution resulting in lower fusion power. In particular, high-Z impurity accumulation, predicted by collisional transport theory, may be devastating for fusion experiments. However the presence of impurities at the edge can be beneficial, and it is planned to seed impurities at the edge of the plasma in future fusion devices to create an edge-localized radiation belt for continuous heat exhaust.[1] It is therefore very important to understand the impurity transport so that accumulation in the core can be avoided. Models of impurity transport driven by microturbulence[2–9] and neoclassical processes[10–12] are now well developed, but there are still many open issues regarding the sign and magnitude of the impurity transport and its parametric dependencies. One example of this is the experimental observation that the direction of impurity flux depends on the auxiliary heating.[13–15] The physical mechanism by which the change of the direction of the impurity convective flux occurs has not yet been clearly identified, in spite of the attempts that has been made.[3,4] When attempting to solve these issues, it is important to know when sophisticated theoretical models are needed and when it is reasonable to apply reduced models to interpret the results of experiments or numerical simulations.

One of the most used simplifications in impurity transport modeling is the so-called trace impurity approximation. Previous work on impurity transport, see, e.g., Refs. 3, 4, and 7 was mainly based on the trace approximation where the impurity species is neglected in the quasineutrality condition. The resulting trace impurity transport is driven by a background turbulence that is independent of impurity parameters. The trace approximation is expected to fail when the dilution parameter Zf_z is large, where Z is the charge number and $f_z=n_z/n_e$ is the fraction of impurities of the plasma. The impurities will then influence the turbulence by main ion dilution or by excitation of impurity modes.

In the present work, impurity particle transport is studied self-consistently using a fluid model for ion-temperature gradient (ITG) and trapped electron (TE) mode driven transport as well as neoclassical theory. The fluid model used here has shown results in good agreement with gyrokinetic predictions of impurity transport[5] and is well suited for the present study of impurity transport due to its simplicity and tractability. In particular, the validity of the trace impurity approximation is investigated and the scalings of the impurity particle transport with temperature and density gradients, impurity fraction and impurity charge are discussed. Furthermore, the impurity density peaking factor is calculated for zero impurity flux, by balancing the outward diagonal impurity flux with the convective velocity (impurity pinch). Such a zero flux region is relevant to steady state plasmas in the core of tokamaks since the impurity influx occurs through the edge. Comparisons with neoclassical predictions for impurity flux and impurity density peaking factor are presented including an interpretative transport analysis representing typical tokamak parameter values using ITER-like profiles based on ASTRA modeling.[16]

The paper is organized as follows. In Sec. II the theoretical model (fluid and neoclassical) is described. Section III presents a discussion of the impurity transport in trace and self-consistent descriptions, complemented with a comparison with neoclassical impurity transport. In Sec IV the impurity diffusivity is computed for an ITER scenario and finally the conclusions are given in Sec. V.

II. MODEL DESCRIPTION

We assume that the total impurity transport is a sum of turbulence-driven transport and neoclassical transport. The turbulent transport is studied by means of a quasilinear fluid model described in Ref. 5 and the neoclassical transport is computed using NEO described in Ref. 10. NEO solves a hierarchy of equations derived by expanding the drift-kinetic equation in powers of ρ_{*i}, the ratio of the ion gyroradius to the system size. The collision operator used for the calculations in this paper is the zeroth-order Hirshman–Sigmar

model, which for the impurity particle fluxes, gives satisfactory agreement with the full Hirshman–Sigmar operator unless the plasma is deep into the collisional regime.

For the turbulent transport we use two different versions of the quasilinear fluid model in the collisionless electrostatic limit. The quasilinear fluid model is based on the solution of a set of fluid equations for the perturbations in density n_j, parallel velocity $v_{\|j}$, and temperature T_j, for ions, impurities, and trapped electrons,[17]

$$\frac{\partial n_j}{\partial t} + \nabla \cdot (n_j \boldsymbol{v}_j) = 0, \tag{1}$$

$$m_{i,z} n_{i,z} \frac{\partial v_{\|i,z}}{\partial t} + \nabla_\| (n_{i,z} T_{i,z}) + n_{i,z} e \nabla_\| \phi = 0, \tag{2}$$

$$\frac{3}{2} n_j \frac{dT_j}{dt} + n_j T_j \nabla \cdot \boldsymbol{v}_j + \nabla \cdot \boldsymbol{q}_j = 0, \tag{3}$$

where $j=i,z,et$ represent ions, impurities, and trapped electrons, $\boldsymbol{v}_j=\boldsymbol{v}_E+\boldsymbol{v}_{*j}+\boldsymbol{v}_{pj}+\boldsymbol{v}_{\pi j}$, $\boldsymbol{v}_E$ is the $\boldsymbol{E}\times\boldsymbol{B}$ velocity, $\boldsymbol{v}_{*j}$ is the diamagnetic drift velocity, $\boldsymbol{v}_{pj}$ is the polarization drift velocity, $\boldsymbol{v}_{\pi j}$ is the drift due to the off-diagonal elements of the stress tensor, and $\boldsymbol{q}_j$ is the diamagnetic heat flux. The closure of the fluid equations is obtained by assuming that the heat flux is equal to the diamagnetic heat flux for all particle species. The free electrons are assumed adiabatic $\delta n_{ef}/n_{ef}=e\phi/T_e$. Assuming quasineutrality, $\delta n_e/n_e=(1-Zf_z)\delta n_i/n_i+Zf_z\delta n_z/n_z$, where $f_z=n_z/n_e$ is the impurity fraction, a closed set of equations is obtained.

The quasilinear particle fluxes are computed from $\Gamma_{nj}=\langle \delta n_j \boldsymbol{v}_{Ej}\rangle$, which is summed over all unstable modes for a fixed space scale of the turbulence, with $k_r\rho_s=k_\theta\rho_s$, where r and θ are radial and poloidal coordinates, $\rho_s=c_s/\Omega_{ci}$, $c_s=\sqrt{T_e/m_i}$ is the sound speed and Ω_{ci} is the cyclotron frequency. The saturation level of the electrostatic potential is estimated by balancing the linear growth with the dominant convective nonlinearity in the energy and continuity equations. In the trace impurity approximation, the trace species is neglected in the quasineutrality condition ($Zf_z\to 0$). The trace impurity flux then becomes linear in the impurity density gradient and can be written as $\Gamma_{nz}=-D_z\partial n_z/\partial r+V_z n_z$, where D_z and V_z are the impurity density and convective velocity, respectively. The impurity density peaking factor normalized to the major radius $-R\nabla n_z/n_z=R/L_{nz}$ is calculated numerically from the condition of zero impurity flux $\Gamma_z=0$. In the trace impurity approximation, the peaking factor can be obtained as $R/L_{nz}=-RV_z/D_z$. In the present study, the trace impurity results will be obtained from the condition $\Gamma_z=0$, by using $f_z=10^{-4}$ in Eqs. (1)–(3). If Zf_z is not small, the trace impurity approximation will not give reliable results. In this case the effect of impurities may be approximated by including the dilution of the main ions $(1-Zf_z)$ in the quasineutrality condition, but neglecting the impurity response $Zf_z\delta n_z/n_z$. The trace as well as the dilution approximation will in the following be compared to the results of the self-consistent treatment.

The simpler version of this model uses a strong ballooning approximation for the electrostatic potential, valid in a region where the magnetic shear is of order unity. The more comprehensive version employs an eigenfunction with general mode width.

A. Strong ballooning approximation

The eigenvalue equation is reduced to a set of algebraic equations using the semilocal analysis of Ref. 18 where the norms $\langle k_\|^2\rangle, \langle k_\perp^2\rangle, \langle \omega_{Di,z}\rangle$, with $\langle\cdots\rangle=\int_{-\pi}^{\pi}\phi(\cdots)\phi d\theta$, are calculated using a strongly ballooning eigenfunction. The solution of the eigenvalue problem gives the eigenvalues and the perturbations in density, temperature, and parallel velocity in terms of the perturbed electrostatic potential. Here, the trapped electron magnetic drift is, after bounce averaging, replaced by the precession frequency of trapped electrons as $\langle\omega_{De}\rangle=\omega_{De}\lambda_t$ with $\lambda_t=1/4+2s/3$,[19] where $s=(r/q)dq/dr$ and q is the safety factor. The space scale of the turbulence is usually assumed to be fixed at $k_r\rho_s=k_\theta\rho_s=0.3$, corresponding to the scale of the fastest growing mode. The sensitivity of the results to the choice of $k_r\rho_s$ will also be discussed. The strong ballooning approximation has recently been shown to give results in good agreement with the results of calculations based on an eigenfunction with general mode width and with gyrokinetic simulations,[5] but its validity breaks down in regions of very low shear, where the eigenfunction diverges.

B. Eigenfunction with general mode width

In the ITER scenario treated in Sec. IV, the magnetic shear is very low throughout the central part of the plasma. In this region, the assumptions of the strong ballooning model break down, and in order to treat the transition from strong to weak ballooning in regions of weak magnetic shear, the eigenvalue equation is solved for an electrostatic potential of general mode width (see Ref. 5 and references therein). The model is based on the same set of equations [Eqs. (1)–(3)] as used in the strong ballooning analysis but the eigenfunction is assumed to be a Gaussian with $\phi\propto\exp(-\alpha\theta^2)$, where θ is the extended poloidal angle and α depends on the plasma parameters and eigenvalues. The curvature terms ω_{Dj} and parallel wavenumber $k_\|$ are evaluated as averages over the eigenfunction. The space scale of the turbulence is here assumed to be $k_r\rho_s=k_\theta\rho_s=0.2$, to match the wave number of the dominant mode as computed by the nonlinear gyrokinetic code GYRO (Ref. 20) for the selected ITER scenario, see Ref. 21 for details.

The turbulent part of the impurity transport is driven mainly by diffusion, thermodiffusion, curvature, and parallel compression. In the trace approximation, without impurity finite Larmor radius effects, the expression for the impurity particle flux is[4]

$$\Gamma_z = 2\bar{\gamma}^3 \frac{n_z}{L_{nz}} \frac{\rho_s c_s}{R k_\theta |\bar{N}_z|^2} (\Delta_1 - \Delta_T \eta_z - 2\Delta_2 L_{nz}/R - Q_\| \Delta_\|), \tag{4}$$

where γ is the linear growth rate of the unstable mode, the overbar denotes normalization with respect to the electron magnetic drift frequency $\omega_{De}=2k_\theta T_e/eBR$, $L_{na}=-n_a/n_a'$ and $L_{Ta}=-T_a/T_a'$ are the density and temperature scale lengths for particle species a, $\eta_z=L_{nz}/L_{Tz}$, $|\bar{N}_z|^2=N_{zr}^2+N_{zi}^2$, with N_{zr}

$=(\bar{\omega}_r+5\tau_z/3)^2-\bar{\gamma}^2-10\tau_z^2/9$ and $N_{zi}=2\bar{\gamma}(\bar{\omega}_r+5\tau_z/3)$, ω_r is the real frequency of the unstable mode, and $\tau_z=T_z/ZT_e$. The diffusion associated with $\Delta_1=[(\bar{\omega}_r+7\tau_z/3)^2+\bar{\gamma}^2+6\tau_z^2/9]$ is always outward. The thermodiffusion associated with $\Delta_T=2\tau_z(\bar{\omega}_r+5\tau_z/3)$ is inversely proportional to the charge number Z and changes sign with $\bar{\omega}_r+5\tau_z/3$. It is therefore outward for instabilities rotating in the ion drift direction (ITG) and inward for those rotating in the electron drift direction (TE). The curvature drift associated with $\Delta_2=[(\bar{\omega}_r+5\tau_z/3)^2+\bar{\gamma}^2+10\tau_z^2/9]$ is inward regardless the sign of the real frequency of the mode and it usually dominates. The parallel dynamics associated with the last term, where $Q_\parallel=Z/[A_z(2qk_\theta\rho_s)^2|N_1|^2]$, $N_1=\bar{\omega}_r-2\tau_z$, and $\Delta_\parallel=2\bar{\omega}_r|\bar{\omega}|^2+\tau_z(19\bar{\omega}_r^2/3-\bar{\gamma}^2/3+100\tau_z\bar{\omega}_r/9-5\tau_z^2)$ leads to a drift that is directed inward for instabilities rotating in the ion drift direction and outward for those rotating in the electron drift direction.[3]

III. RESULTS

The normalized impurity particle flux $R\Gamma_z/n_z$ and peaking factor R/L_{nz} have been studied in two cases: an ITG-dominated case with a large normalized ion temperature gradient, and a TE mode dominated case, where the ion temperature gradient R/L_{Ti} was set to zero. In the studied cases we assume safety factor $q=1.4$, magnetic shear $s=0.8$, fraction of trapped electrons $f_t=0.5$, equal electron, ion, and impurity temperatures $T_e/T_{i,z}=1$, normalized electron density gradient $R/L_{ne}=3$, fixed space scale of the turbulence $k_r\rho_s=0.3$, and the impurity charge $Z=6$, $A_z=12$ unless otherwise specified. For these parameters, the ITG-mode is the dominant instability for large ion temperature gradients, whereas the TE mode dominates for weak ion temperature gradients.

First, we illustrate the sensitivity of the impurity peaking factor in the trace impurity limit to the space scale of the turbulence by varying the correlation length $k_r\rho_s$ from 0.2 to 0.4. Then we discuss the scaling of the impurity peaking factor with impurity charge Z and impurity fraction f_z, both in the ITG and the TE mode dominated cases, compared to the neoclassical peaking factor. Finally, the scalings of the impurity flux and peaking factor with the background temperature and impurity density gradient are shown, and the trace model is compared with the dilution model and the predictions of the self-consistent calculations. In this section, the strong ballooning version of the fluid model has been used, and the results are compared to the neoclassical flux computed by NEO for typical tokamak parameters, with ion density $n_i=5\times10^{19}$ m^{-3}, temperature $T_{i,e,z}=5$ keV, minor radius $a=1$ m, and major radius $R=3$ m.

A. *Z*-scaling

Figure 1 illustrates the scaling of the turbulent impurity density peaking factor with impurity charge Z and with the space scale of the turbulence ($k_r\rho_s$) as a parameter. Trace levels of impurities are used ($f_z=10^{-4}$) and $k_r\rho_s$ is varied from $k_r\rho_s=0.2$ (solid line) to $k_r\rho_s=0.3$ (dashed line), and $k_r\rho_s=0.4$ (dotted line). In Fig. 1(a), the normalized temperature gradients are $R/L_{Tj}=7$, corresponding to an ITG-dominated regime. The peaking factor increases with Z for low-Z impurities and saturates in the limit of large Z. The reason for this is that the contribution from the thermodiffusive pinch, which is outward in the ITG-dominated case, is reduced for large Z.[3] The sign of the impurity pinch is inward, and the Z scaling of the peaking factor is qualitatively similar for the considered $k_r\rho_s$ values. In Fig. 1(b), a TE mode dominated case is considered with $R/L_{Ti}=0$ and the other parameters, as in Fig. 1(a). We note that the Z-scaling is reversed as compared to Fig. 1(a) since the thermodiffusive pinch is inward in this case. Here, a qualitative change occurs for small values of $k_r\rho_s$ where the impurity pinch changes sign from inward to outward, resulting in a negative peaking factor. A flatter electron density profile with $R/L_{ne}=0.5$ gives similar results. In that case the difference between $k_r\rho_s=0.2$ and $k_r\rho_s=0.3$ is even more pronounced because the peaking factors for $k_r\rho_s=0.2$ vary between $R/L_{nz}=-0.66$ for $Z=6$ to $R/L_{nz}=-0.78$ for $Z=60$, while the peaking factors in the other cases are approximately the same as in the peaked density case. In these cases the peaking factor changes sign due to the parallel compression term associated with $\Delta_\parallel$ in Eq. (4). This term is outward for TE modes and can overcome the curvature and thermodiffusive parts of the transport for sufficiently low $k_r\rho_s$. Such a change in the direction of the impurity pinch has been observed in experiments when radio frequency heating is deposited on the electrons.[13–15]

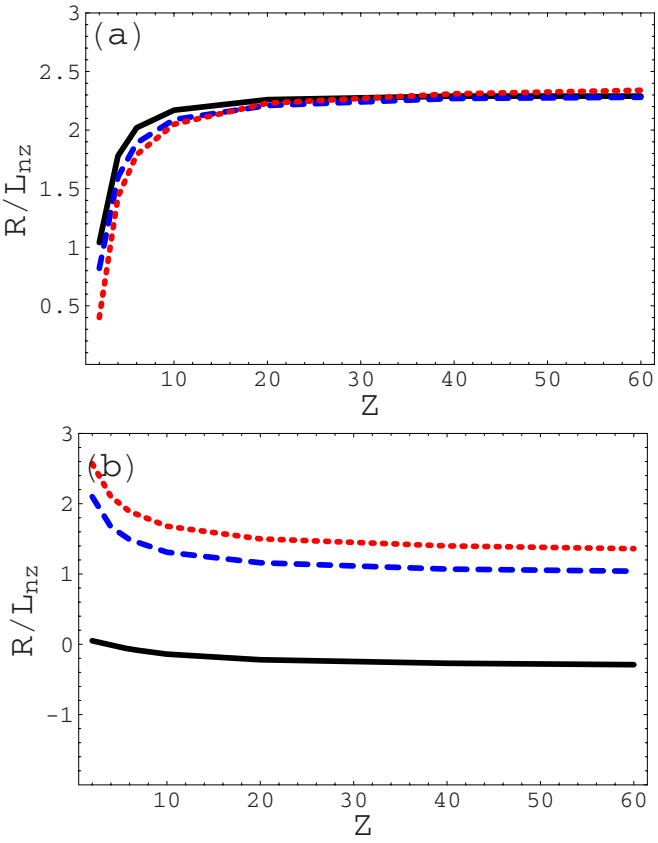

FIG. 1. (Color online) Impurity density peaking factor R/L_{nz} vs charge number Z for $k_r\rho_s=0.2$ (solid line), $k_r\rho_s=0.3$ (dashed line), and $k_r\rho_s=0.4$ (dotted line). The other parameters are $q=1.4$, $s=0.8$, $f_t=0.5$, $T_e/T_{i,z}=1$, and $R/L_{ne}=3$. (a) ITG-dominated case for $R/L_{Tj}=7$. (b) TE dominated case for $R/L_{Te,z}=7$ and $R/L_{Ti}=0$.

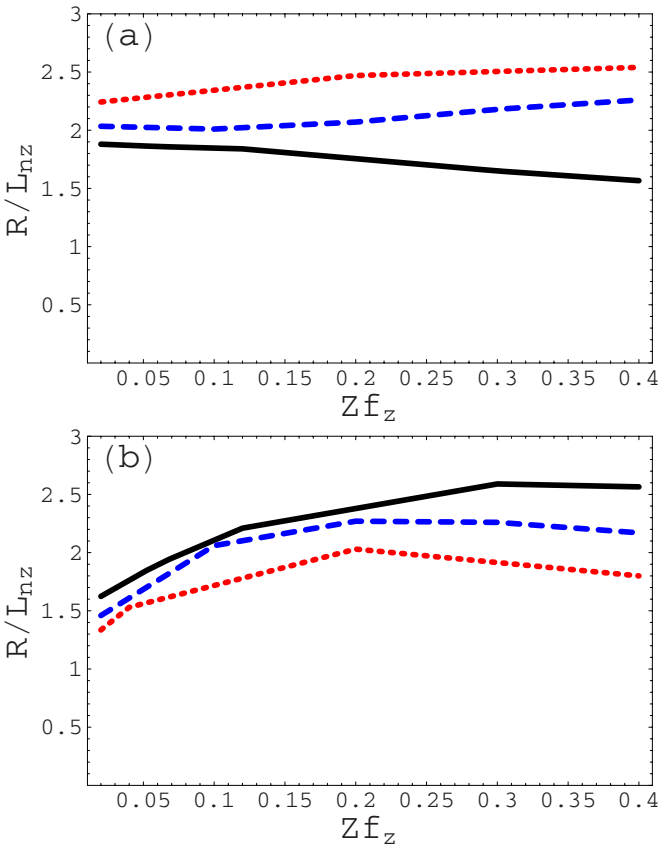

FIG. 2. (Color online) Turbulent impurity density peaking factor R/L_{nz} vs dilution factor Zf_z for $Z=6$ (solid line), $Z=10$ (dashed line), and $Z=20$ (dotted line). The other parameters are the same as in Fig. 1 and $k_r\rho_s=0.3$. (a) ITG-dominated case for $R/L_{Tj}=7$. (b) TE dominated case for $R/L_{Te,z}=7$ and $R/L_{Ti}=0$.

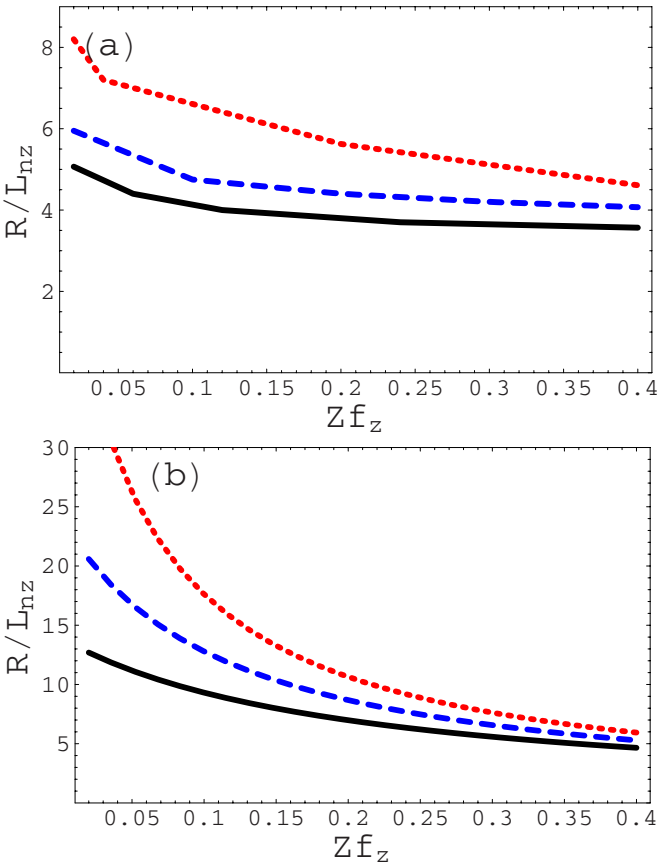

FIG. 3. (Color online) Neoclassical impurity density peaking factor R/L_{nz} versus dilution factor Zf_z for $Z=6$ (solid line), $Z=10$ (dashed line), and $Z=20$ (dotted line). The other parameters are the same as in Fig. 2. (a) ITG-dominated case for $R/L_{Tj}=7$. (b) TE dominated case for $R/L_{Te,z}=7$ and $R/L_{Ti}=0$.

However, in the present case where the sign of the impurity pinch depends on $k_r\rho_s$, a reliable prediction would require a turbulence simulation which follows the nonlinear evolution of the length scales and calculates their total contribution to the pinch.

In Fig. 2 the turbulent impurity density peaking factor R/L_{nz} versus the dilution factor Zf_z is illustrated for $Z=6$, $Z=10$, and $Z=20$. Above $Z=20$ the peaking factor is only weakly dependent of Z, see Fig. 1. The parameters of Fig. 2(a) are $R/L_{Tj}=7$, corresponding to an ITG-dominated regime. The parameters of Fig. 2(b) are $R/L_{Ti}=0$ and $R/L_{Tz}=R/L_{Te}=7$, corresponding to a TE mode dominated regime. In the ITG-dominated regime the peaking factor is very weakly dependent on f_z, while in the TE mode dominated regime, the increase in the peaking factor with f_z is more substantial and it is due to the impurity ITG-mode, which gives a non-negligible contribution to the inward transport in the ITG stable regime ($\nabla T_i=0$). The peaking factor shows a slight decrease for large impurity concentration because the real frequency of the TE mode (which gives the largest contribution to the transport) changes as the impurity concentration increases.

Figure 3 shows the neoclassical impurity density peaking factor that is obtained by varying R/L_{nz} until the neoclassical impurity flux is zero. The parameters are the same as in Fig. 2. The neoclassical peaking factor is determined by a competition between the inward pinch driven by the density gradient and impurity temperature gradient and the outward flux driven by the ion temperature gradient. For the assumed parameters, the inward flux dominates in both ITG and TE mode dominated regimes, and therefore the impurity peaking factor is positive. The peaking factor is larger in the TE mode dominated regime [Fig. 2(d)] than in the ITG-dominated regime because the temperature screening is turned off by setting $R/L_{Ti}=0$ in the former case. The peaking factor decreases with Zf_z since the dilution and the effect of temperature screening change with f_z. In the TE mode dominated case, where the decrease occurs only due to dilution, the peaking factor is proportional to $1/[1+Z(Z-1)f_z]$. The magnitude of the peaking factor increases with Z since the terms driving the major part of the impurity flux (background density and temperature gradients) are Z times larger than the term due to the impurity density gradient.

The neoclassical peaking factor is usually much larger than the turbulent peaking factor. This means that in advanced scenarios, when the turbulence is suppressed and the impurity concentration is very low we would expect a high impurity peaking factor. This is consistent with experimental observations,[22] showing that the impurity density peaking factor is larger in the core than at outer radii and it increases

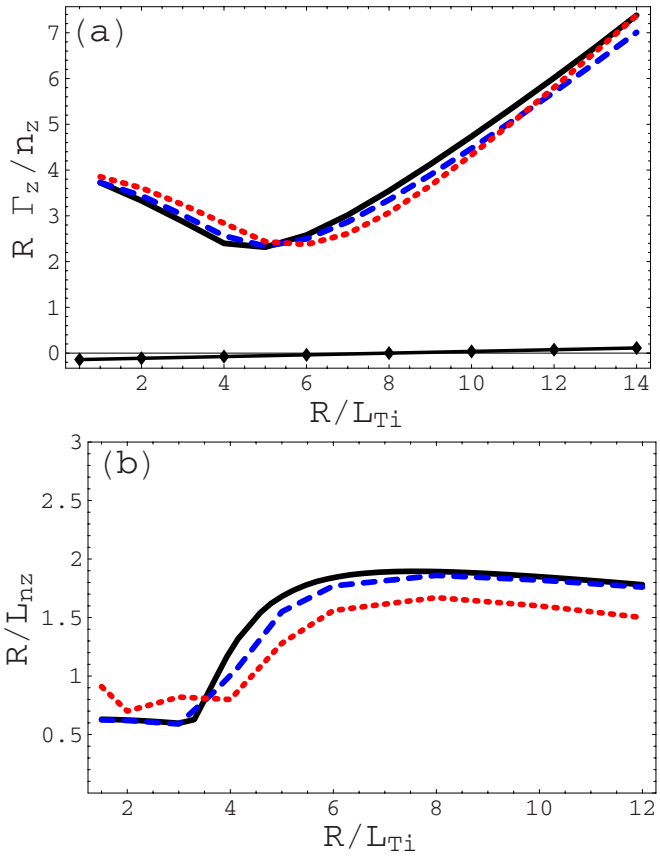

FIG. 4. (Color online) ITG-dominated case for $R/L_{Te}=7$. The other parameters are the same as in Fig. 2. (a) Normalized turbulent impurity particle flux $R\Gamma_z/n_z$ in units of $2\rho_s^2 c_s/R$ vs $R/L_{Ti}=R/L_{Tz}$ for $R/L_{nz}=3$ with $f_z=10^{-4}$ (solid line), $f_z=0.02$ (dashed line), and $f_z=0.05$ (dotted line). The neoclassical flux is shown by diamonds for $f_z=0.02$. (b) Impurity density peaking factor R/L_{nz} vs $R/L_{Ti}=R/L_{Tz}$ for varying impurity fraction. The ITG stability threshold is at $R/L_{Ti}=3.3$ and coincides with the sudden increase in the peaking factors in (b).

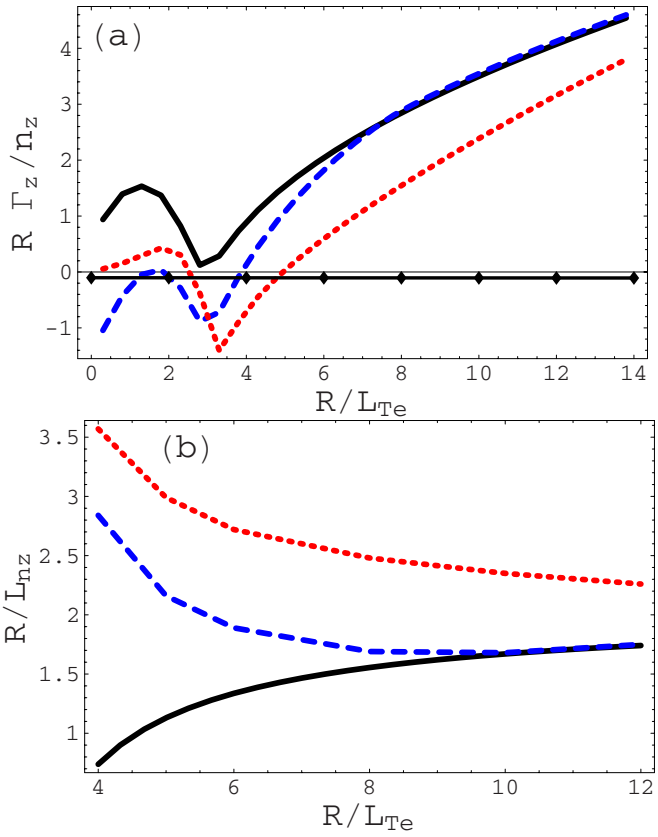

FIG. 5. (Color online) TE dominated case for $R/L_{Ti}=0$ and $R/L_{Tz}=7$. The other parameters are the same as in Fig. 2. (a) Normalized impurity particle flux $R\Gamma_z/n_z$ in units of $2\rho_s^2 c_s/R$ vs R/L_{Te} for $R/L_{nz}=3$ with $f_z=10^{-4}$ (solid line), $f_z=0.02$ (dashed line), and $f_z=0.05$ (dotted line). The neoclassical flux is shown by diamonds for $f_z=0.02$. (b) Impurity density peaking factor R/L_{nz} vs R/L_{Te} for varying impurity fraction.

with Z. Note that for flat density profiles, temperature screening will dominate, and the peaking factor can become negative.

B. R/L_T-scaling

Figure 4(a) shows the normalized impurity particle flux $R\Gamma_z/n_z$ (in units of $2\rho_s^2 c_s/R$) as a function of the ion/impurity temperature gradient parameter $R/L_{Ti}=R/L_{Tz}$ for various impurity fractions: $f_z=10^{-4}$ (trace, solid line), $f_z=0.02$ (dashed line), and $f_z=0.05$ (dotted line). The normalized impurity density and electron temperature scale lengths are $R/L_{nz}=3$ and $R/L_{Te}=7$. Figure 4(b) shows the turbulent impurity density peaking factor R/L_{nz} corresponding to the condition of zero impurity flux with the other parameters as in Fig. 4(a). The impurity density peaking factor [Fig. 4(b)] is significantly smaller in the small $R/L_{Ti,z}$ regime, where the transport driven by TE modes is more important. This is mainly a result of parallel impurity compression which contributes to an outward impurity convective velocity for TE modes.[3] Also here, the increase in the peaking factor with f_z obtained for small values of $R/L_{Ti,z}$ is driven by the impurity ITG-mode, which is neglected in the trace impurity approximation and which gives a non-negligible contribution to the impurity flux below the ITG stability threshold. The fact that this mode exists for low values of $R/L_{Ti,z}$ has been pointed out in Ref. 9. The decrease in the peaking factor with increasing impurity fraction f_z for large $R/L_{Ti,z}$ is a result of the stabilization of the ITG-mode for increasing impurity fraction f_z, mainly due to main ion dilution.

Figures 5(a) and 5(b) show the normalized impurity particle flux $R\Gamma_z/n_z$ (in units of $2\rho_s^2 c_s/R$) and the normalized impurity density peaking factor R/L_{nz} as a function of the electron temperature gradient parameter R/L_{Te} for $f_z=10^{-4}$ (trace, solid line), $f_z=0.02$ (dashed line), and $f_z=0.05$ (dotted line). The other parameters are $R/L_{nz}=3$, $R/L_{Ti}=0$, and $R/L_{Tz}=7$ corresponding to a TE mode dominant regime. In this case, the increasing impurity concentration has a dramatic effect, especially on the peaking factor. This is a result of the impurity ITG-mode which rotates in the same direction as the main ITG-mode and therefore tends to increase the peaking factor. The impurity ITG-mode is now competing with the TE mode since the main ITG-mode is stable, and therefore it has a larger influence than in Fig. 4(b).

The neoclassical flux is considerably smaller and is shown by lines with diamonds for $f_z=0.02$ in Figs. 4(a) and 5(a). The neoclassical flux is inward for low temperature

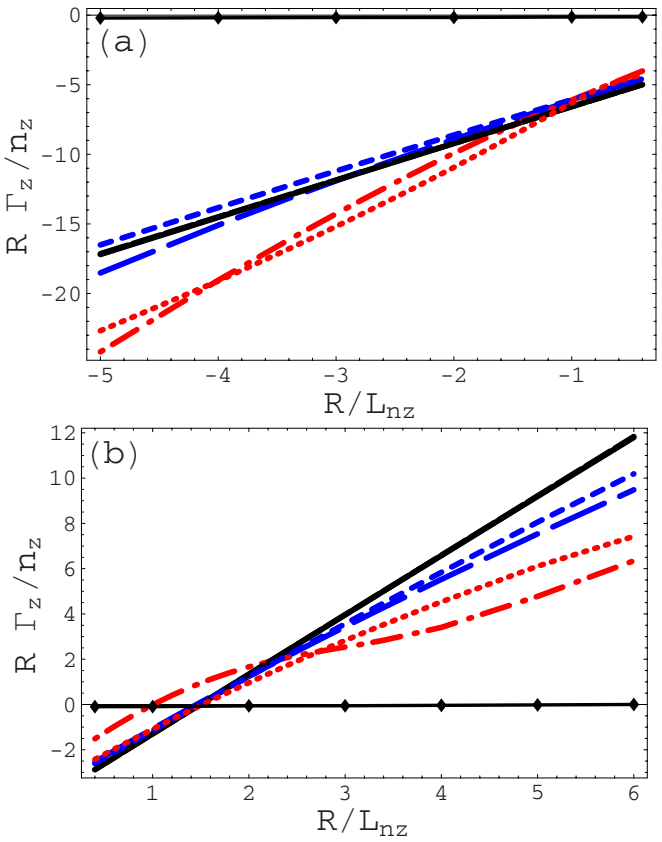

FIG. 6. (Color online) Normalized impurity particle flux $R\Gamma_z/n_z$ in units of $2\rho_s^2 c_s/R$ vs R/L_{nz} for $f_z=10^{-4}$ (black solid line), $f_z=0.02$ (blue long-dashed and short-dashed lines), $f_z=0.05$ (red dotted and dashed-dotted lines). The other parameters are $q=1.4$, $s=0.5$, $f_t=0.5$, $k_r\rho_s=0.3$, $T_i/T_{e,z}=1$, $R/L_{ne}=3$, and $R/L_{Tj}=5$. The results of the dilution model (short-dashed and dotted lines) are compared to the self-consistent model (long-dashed and dashed-dotted lines). The neoclassical flux is shown by lines with diamonds for $f_z=0.02$.

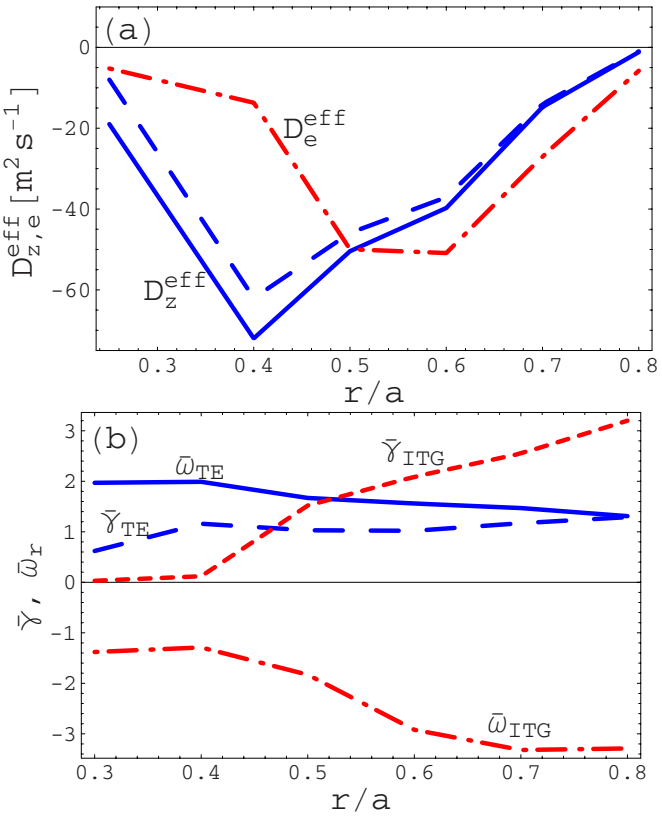

FIG. 7. (Color online) (a) Particle diffusivities vs normalized radius r/a for an ITER-like scenario from the quasilinear fluid model: D_z^{eff} for $Z=6$ (blue solid and dashed lines) and D_e^{eff} (red dashed-dotted line). Solid line is the self-consistent result and dashed line is the trace impurity approximation. (b) Real part of the eigenfrequencies $\bar{\omega}_r$ (solid and dashed-dotted lines) and growth rates $\bar{\gamma}$ (long and short-dashed lines) of the unstable modes, normalized to ω_{De}.

gradients, but changes sign, as the effect of temperature screening becomes more pronounced for larger temperature gradients.

C. R/L_{nz}-scaling

Figure 6 displays the normalized impurity particle flux $R\Gamma_z/n_z$ (in units of $2\rho_s^2 c_s/R$) versus the normalized impurity density gradient R/L_{nz} for negative [Fig. 6(a)] and positive [Fig. 6(b)] values of R/L_{nz} with the impurity fraction f_z as a parameter. The impurity fraction is $f_z=10^{-4}$ (black line), $f_z=0.02$ (blue long-dashed and short-dashed lines), and $f_z=0.05$ (red dotted and dashed-dotted lines) and the other parameters are $R/L_{Tj}=5$ and $s=0.5$. The results of the self-consistent treatment (solid line), neglecting the parallel dynamics for simplicity, are compared with the results of a dilution model (dashed line) which includes the dilution factor $(1-Zf_z)$ in the quasineutrality condition while neglecting the impurity response in the charge balance. The dilution effect is apparent as larger f_z results in a lower impurity flux compared to the trace result. This effect is well reproduced by the dilution model (dashed line). For larger values of f_z however, the impurity ITG-mode is excited and a self-consistent treatment is needed. For $Z=6$ the trace impurity model gives qualitatively correct results if $f_z<0.02$, where $f_z=n_z/n_e$. The dilution model gives a fair agreement up to $f_z<0.05$. The neoclassical flux is given by diamonds for $f_z=0.02$ and also here it is much smaller than the turbulent flux.

IV. ITER-LIKE SCENARIO

In order to illustrate the anomalous impurity flux for ITER-like parameters and compare the trace and the self-consistent treatment, a specific ITER scenario[16] is studied. The selected scenario is a hybrid mode obtained with the ASTRA code, with a plasma current of 12 MA, major radius $R=6.2$ m, minor radius $a=2$ m, and magnetic field $B=5.3$ T. The density profiles are flat and impurity and ion temperatures are assumed equal, and the parameters we used are given in Ref. 21.

The turbulent impurity flux for $Z=6$ is calculated using the quasilinear fluid model in the weak-ballooning limit assuming $k_r\rho_s=0.2$ and it is compared to the results of trace impurity approximation. Figure 7(a) shows the effective impurity diffusivities (solid and dashed lines are the self-consistent and trace models, respectively) and effective electron diffusivities (dashed-dotted line) from the quasilinear fluid model. These are in good agreement with the results of nonlinear gyrokinetic simulations with GYRO, presented in

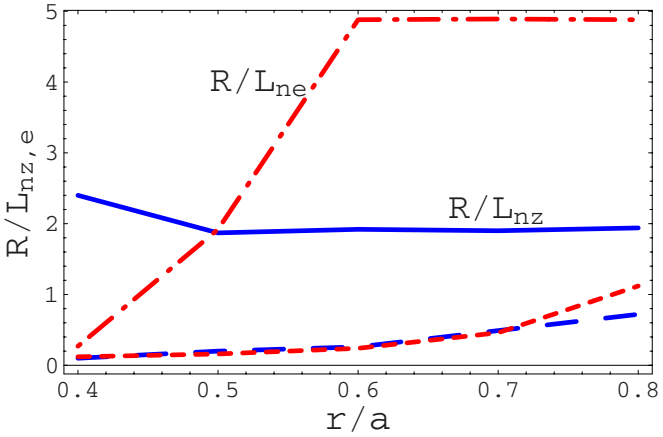

FIG. 8. (Color online) Impurity and electron density peaking factors vs normalized radius r/a for an ITER-like scenario, corresponding to Fig. 7. Solid (blue) and dashed-dotted (red) lines are the impurity and electron peaking factors calculated for given ITER temperature profiles. Long-dashed (blue) and short-dashed (red) lines are the impurity and electron peaking factors corresponding to the assumed density profiles from ASTRA modeling.

Ref. 21. The neoclassical transport for this ITER scenario has been found to be much lower than the turbulent transport.[21] The growth rates and real frequencies of the ITG (red short-dashed and dashed-dotted lines) and TE (blue long-dashed and solid lines) modes for this particular scenario are given in Fig. 7(b). The ITG-mode dominates outside $r/a>0.5$ and TE mode dominates in the core for $r/a<0.4$. The turbulent flux is strongest in the central part of the plasma. Both the electron and impurity particle transport are inward for this ITER scenario but there is significantly weaker transport in the core region where the ITG-mode is stabilized. The trace approximation agrees well with the self-consistent result since $f_z<0.02$, although in the core, where the plasma is TE mode dominated, the deviation from the self-consistent result becomes larger. For the electron diffusivity the trace and self-consistent results coincide.

The effective diffusivities obtained for the selected ITER scenario are very large, mainly due to the assumed strong temperature gradients. Keeping the temperature profiles from the ITER-like scenario fixed, we can calculate the density peaking factors corresponding to the effective diffusivities given by the quasilinear fluid model, assuming zero particle flux. The resulting density peaking factors are considerably larger than the ones obtained from the assumed profiles, as illustrated in Fig. 8, and the electron density profiles are substantially more peaked than the impurity profiles for $r/a>0.5$. However, considering the sensitivity of peaking factors to the temperature gradients (Fig. 4), these results should be complemented by self-consistent calculations of particle and heat fluxes including all the sources and sinks, which is outside the scope of this work.

V. CONCLUSIONS

Comparisons between trace and self-consistent impurity transport and neoclassical predictions have been performed using an electrostatic fluid model for main ion and impurity temperature gradient mode and trapped electron mode turbulence in the collisionless limit. The impurity flux and the impurity density peaking factor have been calculated in both ITG and TE mode dominated cases and their dependence on impurity charge, fraction of impurities, temperature and density gradients, and space scale of the turbulence has been studied and compared to the predictions of neoclassical theory.

As expected, the neoclassical transport is much smaller than the turbulent transport, especially in cases when the density and temperature driven neoclassical fluxes nearly cancel. Therefore neoclassical transport is not expected to influence the impurity density peaking factor unless the turbulence is suppressed. However in advanced scenarios, when the ITG and TE modes are stable, the impurity dynamics will be governed by neoclassical effects. In these cases the impurity peaking factor is usually very large, especially for flat ion temperature gradients, when the effect of temperature screening is small. The neoclassical peaking factor increases with the impurity charge number Z and decreases with the impurity fraction f_z.

In the ITG-mode dominated case the peaking factor is very weakly dependent on the specific value of the space scale of the turbulence $k_r\rho_s$. The peaking factor increases with Z for low-Z impurities and saturates in the limit of large Z. It is only weakly dependent on the dilution parameter Zf_z. The trace impurity model gives qualitatively correct results if $f_z\lesssim 0.02$. The dilution model gives a fair agreement up to $f_z<0.05$. Thus for small impurity concentrations ($f_z\lesssim 0.02$), the trace impurity limit is adequate if the plasma is dominated by ITG turbulence.

In the TE mode dominated plasmas the peaking factor is remarkably sensitive to the choice of $k_r\rho_s$ and even changes sign when varying $k_r\rho_s$ from $k_r\rho_s=0.2$ to $k_r\rho_s=0.3$. Here, the effect of increasing impurity concentration is substantial, and therefore the self-consistently calculated impurity flux and peaking factor can be significantly different from the trace approximation. The difference has been shown to be caused by the impurity ITG-mode, which gives a non-negligible contribution to the transport in the ITG stable regime.

The impurity and electron particle fluxes and density peaking factors have been calculated for an ITER-like profile based on ASTRA modeling. For the considered ITER scenario, the trace impurity approximation gives results in good agreement with the self-consistent treatment due to the low impurity concentration and the electron density peaking factor has been found to be substantially larger than the impurity peaking factor for $r/a>0.5$.

ACKNOWLEDGMENTS

This work was funded by the European Communities under Association Contract between EURATOM and *Vetenskapsrådet*. The views and opinions expressed herein do not necessarily reflect those of the European Commission. The authors would like to thank E. Belli and J. Candy for providing the neoclassical code NEO.

[1] G. P. Maddison, M. Brix, R. Budny, M. Charlet, I. Coffey, J. G. Cordey, P. Dumortier, S. K. Erents, N. C. Hawkes, M. von Hellermann, D. L. Hillis, J. Hogan, L. D. Horton, L. C. Ingesson, S. Jachmich, G. L. Jackson, A.

Kallenbach, H. R. Koslowski, K. D. Lawson, A. Loarte, G. F. Matthews, D. McDonald, G. R. McKee, A. Meigs, A. M. Messiaen, R. Milani, P. Monier-Garbet, M. Murakami, M. F. F. Nave, J. Ongena, M. E. Puiatti, E. Rachlew, J. Rapp, S. Sharapov, G. M. Staebler, M. Stamp, J. D. Strachan, W. Suttrop, G. Telesca, M. Z. Tokar, B. Unterberg, M. Valisa, K.-D. Zastrow, and G. Maddison, Nucl. Fusion **43**, 49 (2003).
[2]C. Estrada-Mila, J. Candy, and R. E. Waltz, Phys. Plasmas **12**, 022305 (2005).
[3]C. Angioni and A. G. Peeters, Phys. Rev. Lett. **96**, 095003 (2006).
[4]H. Nordman, R. Singh, T. Fülöp, L.-G. Eriksson, R. Dumont, J. Anderson, P. Kaw, P. Strand, M. Tokar, and J. Weiland, Phys. Plasmas **15**, 042316 (2008).
[5]H. Nordman, T. Fülöp, J. Candy, P. Strand, and J. Weiland, Phys. Plasmas **14**, 052303 (2007).
[6]N. Dubuit, X. Garbet, T. Parisot, R. Guirlet, and C. Bourdelle, Phys. Plasmas **14**, 042301 (2007).
[7]R. Guirlet, C. Giroud, T. Parisot, M. E. Puiatti, C. Bourdelle, L. Carraro, N. Dubuit, X. Garbet, and P. R. Thomas, Plasma Phys. Controlled Fusion **48**, B63 (2006).
[8]T. Fülöp and J. Weiland, Phys. Plasmas **13**, 112504 (2006).
[9]M. Fröjdh, M. Liljeström, and H. Nordman, Nucl. Fusion **32**, 419 (1992).
[10]E. A. Belli and J. Candy, Plasma Phys. Controlled Fusion **50**, 095010 (2008).
[11]S. P. Hirshman and D. J. Sigmar, Nucl. Fusion **21**, 1079 (1981).
[12]P. Helander and D. J. Sigmar, *Collisional Transport in Magnetized Plasmas* (Cambridge University Press, Cambridge, 2002).
[13]R. Dux, R. Neu, A. G. Peeters, G. Pereverzev, A. Muck, F. Ryter, and J. Stober, Plasma Phys. Controlled Fusion **45**, 1815 (2003).
[14]M. E. Puiatti, M. Valisa, M. Mattioli, T. Bolzonella, A. Bortolon, I. Coffey, R. Dux, M. von Hellermann, P. Monier-Garbet, M. F. F. Nave, and J. Ongena, Plasma Phys. Controlled Fusion **45**, 2011 (2003).
[15]M. E. Puiatti, M. Valisa, C. Angioni, L. Garzotti, P. Mantica, M. Mattioli, L. Carraro, I. Coffey, and C. Sozzi, Phys. Plasmas **13**, 042501 (2006).
[16]A. Polevoi, personal communication (2006).
[17]J. Weiland, *Collective Modes in Inhomogeneous Plasma* (IOP, Bristol, 2000).
[18]A. Hirose, Phys. Fluids B **5**, 230 (1993).
[19]X. Garbet, N. Dubuit, E. Asp, Y. Sarazin, C. Bourdelle, P. Ghendrih, and G. T. Hoang, Phys. Plasmas **12**, 082511 (2005).
[20]J. Candy and R. E. Waltz, J. Comput. Phys. **186**, 545 (2003).
[21]J. Candy, H. Nordman, M. Fahey, T. Fülöp, and E. Belli, in *Proceedings of the 22nd International Atomic Energy Agency Fusion Energy Conference*, Geneva, 2008 (International Atomic Energy Agency, Vienna, 2008), Paper No. TH/P8-28.
[22]C. Giroud, C. Angioni, L. Carraro, I. H. Coffey, J. Hobirk, M. E. Puiatti, M. Valisa, A. D. Whiteford, P. Belo, T. M. Biewer, M. Brix, R. Buttery, E. Joffrin, L. Lauro Taroni, K. Lawson, P. Mantica, A. Meigs, V. Naulin, M. G. O'Mullane, K.-D. Zastrow, and JET-EFDA contributors, in *Proceedings of the 34th European Physical Society Conference on Plasma Physics*, Warsaw, 2007 (European Conference Abstracts, Warsaw, 2007), Vol. 31F, p. 2.049.